Cooperative Supramolecular Block Copolymerization for the Synthesis of Functional Axial Organic Heterostructures

Cooperative Supramolecular Block Copolymerization for the Synthesis of Functional Axial Organic Heterostructures

Aritra Sarkar,[§] Tejmani Behera,[ξ] Ranjan Sasmal,[§] Riccardo Capelli,[†] Charly Empereur-mot,[‡] Jaladhar Mahato,[ξ] Sarit S. Agasti,*[,§] Giovanni M. Pavan,*[,†,‡] Arindam Chowdhury,*[,ξ] and Subi J. George*[,§]

[§] New Chemistry Unit and School of Advanced Materials (SAMat), Jawaharlal Nehru Centre for Advanced Scientific Research (JNCASR), Jakkur, Bangalore, India-560064.

[ξ] Department of Chemistry, Indian Institute of Technology Bombay, Powai, Mumbai, 400076, India.

[†] Department of Applied Science and Technology, Politecnico di Torino, Corso Duca degli Abruzzi24, 10129 Torino, Italy.

[‡] Department of Innovative Technologies, University of Applied Sciences and Arts of Southern Switzerland, Galleria 2, Via Cantonale 2c, CH-6928 Manno, Switzerland.

ABSTRACT: Supramolecular block copolymerzation with optically or electronically complementary monomers provides an attractive bottom-up approach for the non-covalent synthesis of nascent axial organic heterostructures, which promises to deliver useful applications in energy conversion, optoelectronics, and catalysis. However, the synthesis of supramolecular block copolymers (BCPs) constitutes a significant challenge due to the exchange dynamics of non-covalently bound monomers and hence requirs a fine microstructure control. Furthermore, temporal stability of the segmented microstructure is a prerequisite to explore the applications of functional supramolecular BCPs. Herein, we report the cooperative supramolecular block copolymerization of fluorescent monomers in solution under thermodynamic control, for the synthesis of axial organic heterostructures with light-harvesting property. The fluorescent nature of the core-substituted naphthalene diimide (cNDI) monomers enables a detailed spectroscopic probing during the supramolecular block copolymerization process to unravel a nucleation-growth mechanism, similar to that of chain copolymerization for covalent block copolymers. Structured Illumination Microscopy (SIM) imaging of BCP chains characterizes the segmented microstructure and also allows size distribution analysis to reveal the narrow polydispersity (polydispersity index (PDI) ~ 1.1) for the individual block segments. Spectrally-resolved fluorescence microscopy on single block copolymerized organic heterostructures shows energy migration and light-harvesting across the interfaces of linearly connected segments. Molecular dynamics and metadynamics simulations provide useful mechanistic insights into the free-energy of interaction between the monomers as well as into monomer exchange mechanisms and dynamics, which have a crucial impact on determining the copolymer microstructure. Our comprehensive spectroscopic, microscopic and computational analysis provide an unambiguous structural, dynamic and functional characterization of the supramolecular BCPs. The strategy presented here is expected to pave the way for the synthesis of multi-component organic heterostructures for various functions.

Introduction

The field of supramolecular polymers have emerged as an important research topic over the last two decades for the realization of ordered, nanostructured materials with adaptive and reversible functions.[1] Synthesis of supramolecular copolymers,[2] having multiple monomeric components, with microstructural control is considered as the ensuing level of complexity to be addressed for the design of next generation functional supramolecular materials such as organic heterostructures with nanoscale axial heterojunctions or nanostructures with reconfigurable monomer sequence for efficient functional output.[3] Although several synthetic strategies are available to tailor the monomer sequence in covalent copolymers[4], the microstructure control in supramolecular copolymers has been mostly limited to alternate[5], statistical[2a,6], and periodic arrangements[7] of monomers due to the labile nature of its constituent monomers held by non-covalent interactions. On the other hand, supramolecular block copolymers (BCPs)[1b,2a,b] with segmented microstructure containing long sequences of individual monomers would be the most functional and appealing architecture and has been considered as a holy grail for supramolecular chemists due to the monomer dynamics and difficulty in characterizing such structures.[2a]

In a pioneering work, Manners and co-workers have demonstrated supramolecular BCP structures from self-assembled cylindrical micelles of kinetically inert, poly(ferrocenyldimethylsilane) (PFS)-core containing block copolymers, using a crystallization-driven self-assembly (CDSA) approach.[8] This living crystallization methodology allowed the uniform epitaxial growth on kinetically stable seeds, by the sequential addition of soluble macromolecular monomers to construct a plethora of block copolymer architectures.[9] However, supramolecular copolymerization of low molecular weight monomers has been a significant challenge due to the fast exchange of monomers during the non-covalent synthesis and are seldom reported.[10] In an early attempt, Aida and co-workers have demonstrated the seeded growth of hexabenzocoronene (HBC) derived amphiphilic monomers on kinetically stable stacks of electronically complementary HBC monomers to accomplish

supramolecular tri-block nanostructures.[11] Similarly, Takeuchi, Sugiyasu and co-workers have achieved supramolecular BCPs via seeded growth of porphyrin monomers using a solvent-mixing protocol,[12] in a procedure analogous to the CDSA for polymeric micelles.[8,9] To introduce an additional kinetic control for the synthesis of well-defined segmented microstructures, Würthner and co-workers have demonstrated a seed-induced living supramolecular polymerization (LSP)[2b,13,14] approach for the BCP synthesis of core substituted perylenediimide monomers.[15] Well-defined triblock supramolecular polymer architectures were made under kinetic control by introducing metastable states of one of the monomer to the seeds of another. In a similar kinetically controlled approach, we have recently reported supramolecular BCPs of fluorescent cNDI[16] monomers via heterogeneous nucleation triggered seeded supramolecular polymerization.[17] Seeded LSP process under kinetic control, is analogous to the well-established living polymerization techniques[18] for the synthesis of covalent BCPs[4] and hence has the potential for better structural control if the monomer exchange dynamics can be retarded.

Another synthetic approach to realize the covalent block copolymers is via chain-growth copolymerization by modulating the reactivity ratio of the constituting monomers[2a,19], although dispersity control is compromised to a certain extent compared to the living polymerization strategies. An equivalent non-covalent synthetic method would be a cooperative or nucleation-elongation growth supramolecular copolymerization under thermodynamic conditions.[1a,20] However, thermodynamically controlled cooperative supramolecular copolymerization often resulted in statistical,[6] periodic or gradient[21] microstructures rather than the desired block organization of the monomers, due to the lack of fine-tuning in the free energy of hetero- versus homo-monomeric interactions which determines the reactivity ratio.[2a] In a unique manifestation of supramolecular block copolymerization under thermodynamic control, recently Meijer and co-workers obtained supramolecular BCPs[22] by utilizing a balanced mismatch penalty and cooperativity difference between the two triarylamine based monomers.[23] This synthetic strategy for supramolecular BCPs could result in stable segmented microstructures[2a] and hence are ideally suited for exploring various applications.

We envisage that supramolecular block-copolymerization of organic chromophoric monomers with complementary optical or electronic properties would provide an attractive bottom-up strategy for the synthesis of axial heterostructures with designed interfaces and anisotropic energy or electron transport properties[24] potentially useful in photovoltaics, energy conversion and supramolecular electronics.[3,25] Although inorganic axial heterostructures with two dissimilar semi-conducting components are well exploited,[26] the synthesis of analogous organic heterostructures with linear heterojunctions has been a substantial challenge. In a seminal work, Aida and co-workers have shown enhanced energy transport across the linear p-n heterojunctions of HBC derived supramolecular BCPs.[11a] Although Manners and co-workers have elegantly shown an efficient exciton transport through semi-conducting cores[27] and color tunable fluorescent multi-block nanostructures,[28] in supramolecular block micelles, the transport properties through the linear heterojunctions are not yet investigated. This scenario encouraged us to explore the energy-transport properties along the axial heterostructures at the nanoscale, by the synthesis of supramolecular BCPs of π-conjugated monomers with complementary optical properties.

Herein we report the thermodynamically controlled, solution-phase synthesis of supramolecular BCPs of fluorescent cNDI donor and acceptor monomers which have optical complementarity, to facilitate the energy transfer process along the resultant organic heterostructures. Through a comprehensive spectroscopic, computational and microscopic techniques, we unambiguously demonstrate the structural and functional characteristics of these fluorescent, multi-block architectures.

Results and Discussion

Molecular design

Supramolecular block copolymerization in solution under thermodynamic control requires two structurally similar monomers with a cooperative, nucleation-elongation growth mechanism of homopolymerization.[20,22] In order to minimize the structural mismatch between the monomers, we have used cNDI derivatives as the monomers, since its HOMO-LUMO energy levels and the resultant optoelectronic properties can be modulated by the simple core-substitution with heteroatoms having varying donor strengths.[16] In the present study, we have used ethoxy (-OEt) and pentanethiol (-SC_5H_{11}) cNDI derivatives (Figure 1a), which would render green and red fluorescent monomers, respectively that helps to characterize the resultant supramolecular copolymer via spectroscopic probing and fluorescence microscopic visualization. Further, we envisage that the Förster Resonance Energy Transfer (FRET) between green and red monomers can be used to impart functional characteristics to resulting BCPs as light-harvesting axial organic heterostructures (Figure 1b). To facilitate a hydrogen-bonded cooperative supramolecular polymerization we have attached the cNDI π-conjugated derivatives to chiral (S,S)-trans-1,2-bis(amido)-cyclohexane motif and the resultant bischromophoric derivatives (**SS-dithiol** and **SS-diOEt**) are expected to grow by following a nucleation-elongation mechanism (Figure 1a).[29] In addition, the chiral diaminocyclohexane cores are known to induce chirality during the self-assembly to aid the chiroptical probing of the supramolecular copolymerization process.[29b] **SS-dithiol** and **SS-diOEt**[29b] monomers were synthesized (Schemes S1 and S2) and well characterized.

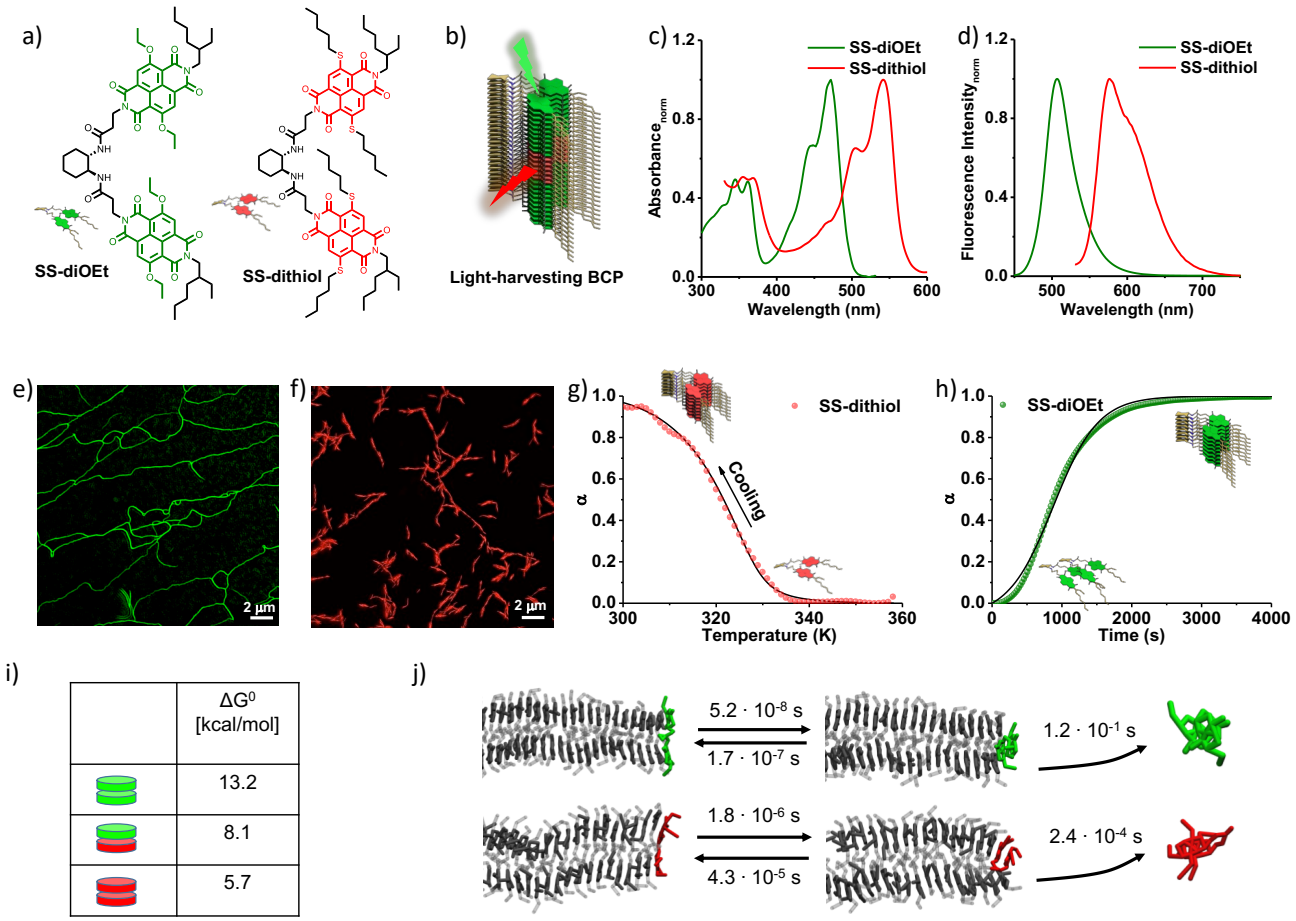

Figure 1. Molecular structures and supramolecular homopolymerization: (a) Molecular structures of **SS-diOEt** and **SS-dithiol** monomers along with its schematic. (b) Schematic representation of light-harvesting axial organic heterostructures (supramolecular BCP) with green-red-green segmented microstructure. Normalized (c) absorption and (d) emission spectra of **SS-diOEt** (λ_{ex} = 430 nm) and **SS-dithiol** (λ_{ex} = 530 nm) homopolymers showing distinct absorption and emission profiles. SIM images of (e) green (green channel) and (f) red (red channel) fluorescent 1D supramolecular homopolymers for **SS-diOEt** and **SS-dithiol**, respectively. (g) Cooling curve depicting the supramolecular homopolymerization of **SS-dithiol** monomers obtained by monitoring the CD changes at 548 nm. The non-linear curve fits well with a nucleation-elongation model (black solid line). The black arrow indicates the direction of cooling. (h) Time-dependent degree of aggregation (α) displaying the transition from the metastable state to supramolecular homopolymers of **SS-diOEt** obtained by monitoring the absorbance change at 370 nm, which could be fitted (black solid line) to an autocatalytic nucleation-elongation growth model. (i) Dimerization/binding free-energies for the **SS-diOEt**/**SS-diOEt**, **SS-diOEt**/**SS-dithiol**, and **SS-dithiol**/**SS-dithiol** interactions. (j) Schematic representation and characteristic timescales (t_{CG}) for the exchange steps involved in the process of monomer exchange from the fiber tips in both **SS-diOEt** (top) and **SS-dithiol** (bottom) supramolecular stacks. Monomer exchange steps: (1) the monomer on the tip, starting from an open/stacked state (left), closes in "sandwich conformation" (middle), and (2) from such closed conformation exchanges with the solution (right). ([**SS-diOEt**] = [**SS-dithiol**] = 2.5×10^{-5} M, TCE/MCH, 25/75 (v/v), l = 10 mm, cooling rate is 1 K/min, (green channel: λ_{ex} = 488 nm, λ_{coll} = 495–575 nm), (red channel: λ_{ex} = 561 nm, λ_{coll} = 570–650 nm)), The homopolymers of **SS-diOEt** and **SS-dithiol** were prepared following Protocol I in experimental procedures.

Mechanistic investigation of supramolecular homopolymerization

Both **SS-diOEt** and **SS-dithiol** monomers remain in its monomeric state in 1,1',2,2'-tetrachloroethane (TCE) (Figure S1 and S5). Supramolecular homopolymerization of these monomers was performed in methylcyclohexane (MCH)/TCE solvent mixtures (TCE/MCH, 40/60 (v/v) to TCE/MCH, 25/75 (v/v)). Samples were prepared by annealing the solutions of respective monomers in appropriate solvent mixtures to 363 K followed by cooling to 298 K a ramping rate of 1 K/min, and the degree of aggregation (α) was monitored at corresponding aggregation spectral features. Combination of absorption, circular dichroism and steady state and time resolved fluorescence spectroscopic studies revealed a J-type slipped organization of chromophores in the supramolecular homopolymers (Figure S1-S5). Distinct absorption (Figure 1c) and emission (Figure 1d) spectral features of stacked **SS-diOEt** and **SS-dithiol** monomers facilitate the independent probing of monomers during the supramolecular copolymerization process (vide infra). The green (λ_{max} = 505 nm) and red (λ_{max} = 575 nm) emission of the **SS-diOEt** and **SS-dithiol** homopolymers (Figures 1c and 1d),

respectively enabled its orthogonal visualization through SIM, as green (Figure 1e and S5) and red-emitting (Figure 1f and S6) supramolecular polymers. Whereas **SS-dithiol** gets excited at both green (λ_{ex} = 488 nm) and red (λ_{ex} = 561 nm) (Figure S7c and 7d), **SS-diOEt** (Figure S7a and 7b) selectively gets excited at the green, facilitating the visualization of supramolecular co-polymers with different microstructure (vide infra).

The cooling curve obtained by monitoring the temperature dependent CD signal changes at 548 nm (Figure S8) for the **SS-dithiol** monomers (c = 2.5×10^{-5} M, TCE/MCH, 25/75 (v/v)) showed a non-linear curve, which could be fitted to a nucleation-elongation model with an elongation temperature (T_e) of 323 K (Figure 1g and S10).[30] On the other hand, **SS-diOEt** monomers in the same solvent composition (2.5×10^{-5} M) while cooling from its monomeric solution at high temperature (Figure S9) to 298 K gets trapped in a metastable state (Figure S11a and S12). However, the metastable state gradually gets converted into a thermodynamically stable supramolecular polymer, as evident from the time-dependent absorption changes at 370 nm (Figure 1h and S11b). Since the CD signal of **SS-diOEt** is contaminated with linear dichroism (LD), the corresponding changes in absorption was probed to follow the self-assembly. Interestingly, the obtained kinetic data could be well-fitted with an autocatalytic Watzky and Finke[31] model suggesting the presence of nucleation-elongation growth mechanism, for **SS-diOEt** monomers (Figure 1h).

Stability and monomer exchange dynamics in supramolecular homopolymers from molecular simulations

I*n silico* investigations based on high-resolution molecular models are important to rationalize the experimental findings, offering a detailed insight into the structural and dynamic behavior of supramolecular polymers.[32] Recently, a combination of metadynamics simulations and fine coarse-grained models allowed to study monomer exchange events that occur within and in/out of the dynamic supramolecular polymers at submolecular resolution.[33] We exploited a similar approach here to explore the relative stabilities, and intrinsic dynamics of **SS-dithiol** and **SS-diOEt** supramolecular homopolymers. first, we developed all atom (AA) and coarse-grained (CG) models for both **SS-dithiol** and **SS-diOEt** monomers (Figure 34) as recently done for similar self-assembling monomers,[17a] the CG models for the systems were developed based on the MARTINI CG force field[34] and have been further refined in order to reproduce the correct behavior of the monomers in the solvent (cyclohexane) seen in the AA models (Section C.1. supporting information).[32b] Using these CG models, we studied the dimerization free-energies (Section C.4. supporting information) associated with the **SS-diOEt/SS-diOEt**, **SS-dithiol/SS-diOEt**, and **SS-dithiol/SS-dithiol** interaction in cyclohexane (Figure 1i: green-green, green-red and red-red dimerization ΔG values, respectively) employing Well-tempered Metadynamics (WT-MetaD)[35] simulations. The obtained ΔG data showed that the most stable interaction is that of the **SS-diOEt** homodimer, followed by the **SS-dithiol/SS-diOEt** heterodimer and the **SS-dithiol** homodimer. This information is useful to rationalize the tendency to monomer mixing during the supramolecular co-polymerization process or following to monomer exchange in/out the supramolecular polymers.

We then built two CG models of pre-formed **SS-dithiol** or **SS-diOEt** supramolecular stacks (fibers) composed of 40 initially extended stacked monomers (Figure 1j). These CG fiber models have been pre-equilibrated using molecular dynamics (MD) simulations (Section c.2. supporting information). We then performed multiple infrequent WT-MetaD simulations biasing the unbinding and exchange of a monomer from the fiber tip into the cyclohexane solvent. We could observe that in both systems the exchange event is characterized by two steps: (1) the monomer closes-up in a "sandwich" conformation and (2) from such closed state, this is released into the solvent (Section C.5. supporting information).[33] We separately characterized step 1 (closing and opening of the tip monomer) and step 2 (release of a closed monomer into the solution) using infrequent MetaD simulations. The obtained transition/exchange timescales for steps (1) and (2) allowed us to reconstruct in a reliable way the kinetics for the monomer exchange.[33] We obtain, for example, information on the characteristic residence times for the monomers on the fibers tips (Figure 1j: t_{CG}). Although such exchange timescales are qualitative (obtained from CG models), these are nonetheless useful to compare the relative dynamics of the two fibers. In particular, exchange step (2) is found slower (less likely) in **SS-diOEt** (t_{CG} ~1.2×10^{-1} s) than in **SS-dithiol** (t_{CG}~2.4×10^{-4} s). Conversely, exchange step 1 is found faster in the **SS-diOEt** (closing/opening timescales, t_{close}/t_{open}, in the order of ~$10^{-8}/10^{-7}$ s) than in the **SS-dithiol** (t_{close}/t_{open} in the order of ~$10^{-6}/10^{-5}$ s). The slower monomer exchange kinetics with the solvent of **SS-diOEt** is in line with the higher **SS-diOEt-SS-diOEt** interaction energies reported in Figure 1i.

In general, in these stacks the closure into the "sandwich" conformation of the monomers at the fibers end appears to be faster than the opening, suggesting that statistically the tips of these stacks are intrinsically more disordered compared to the perfectly organized monomers expected in the fiber bulk. In fact, monomers closure along the fibers introduces defects in these stacks. Such defects are known to be important for the exchange of monomers and overall for the dynamics of the assembly.[33,32b,36] Analysis of the solvent exposure of the individual monomers and of the level of order in these stacks shows that along the **SS-diOEt** fiber more defects are present with respect to **SS-dithiol** fiber (Figure S35). This is interesting, as such defects constitute hot spots from which monomers can exchange in/out the stacks,[32c,33,36] which can lead to the dynamic mixing of monomers. The higher tendency of **SS-diOEt** fiber to be in disordered state compared to **SS-dithiol**, is in agreement with the experimental observation of the entrapment of **SS-diOEt** monomers into local minimum metastable (disordered) states during its temperature-dependent homo-polymerization process. On the other hand, the faster dynamics of **SS-dithiol** assemblies may enable them to reach the thermodynamic equilibrium in a more facile way compared to **SS-diOEt** as observed in the experiment.

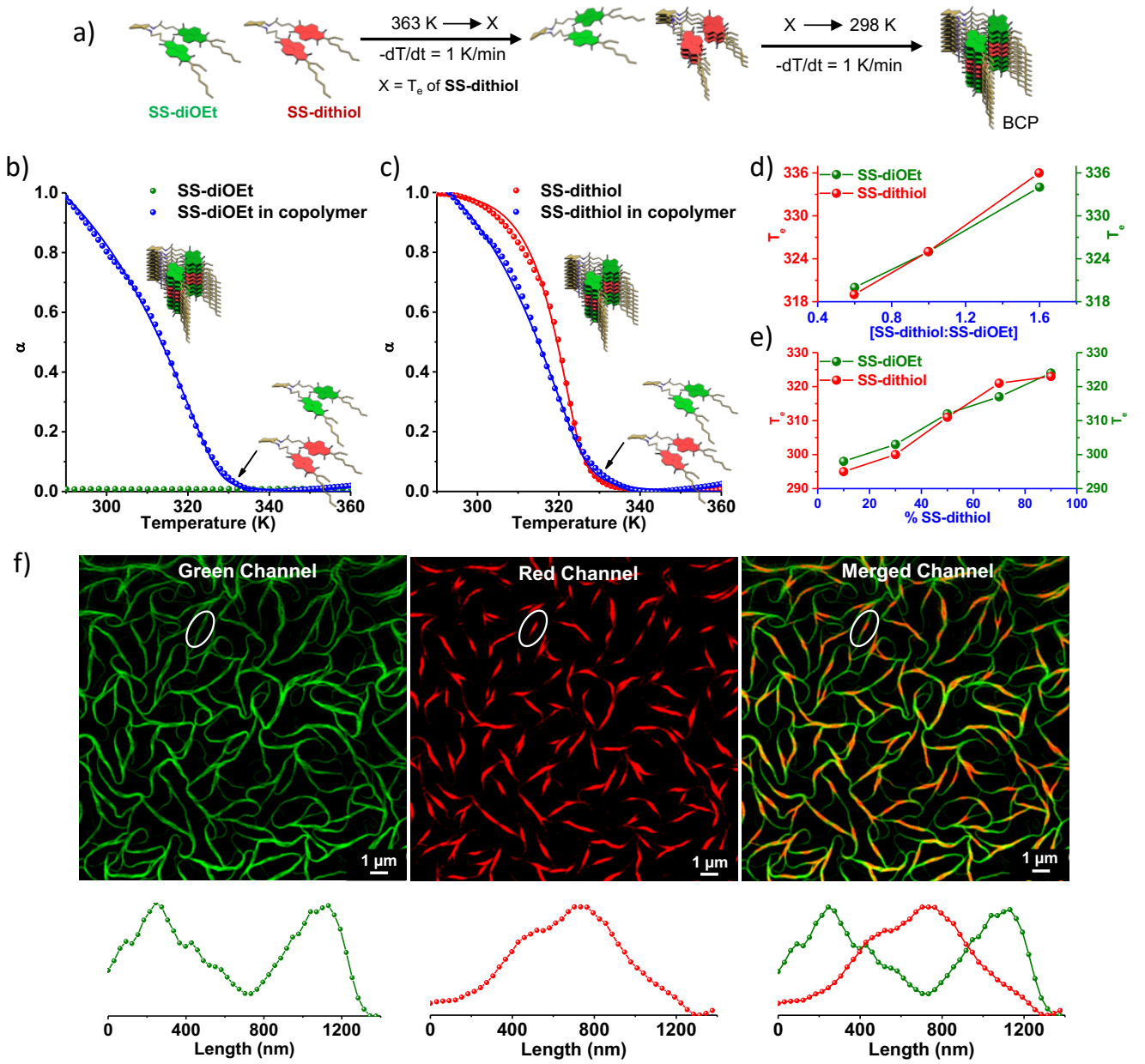

Figure 2. Cooperative Supramolecular Block Copolymerization: (a) Schematic illustration of the supramolecular block copolymerization process, by cooling down a mixture of monomers from high temperature under thermodynamic control. "X" represents the T_e of **SS-dithiol** at a particular concentration which triggers the heterogeneous nucleation of **SS-diOEt** in **SS-dithiol** seeds. Temperature-dependent degree of aggregation (1 K/min cooling rate) obtained by probing the emission changes at (b) 490 nm for **SS-diOEt** (λ_{ex} = 430 nm) and (c) 570 nm for **SS-dithiol** (λ_{ex} = 530 nm), of both homopolymers and BCP, which shows that **SS-diOEt** and **SS-dithiol** elongates at the same temperature confirming a co-assembly process. The elongation temperature (T_e) of the m0nomeric mixture matches well with that of pure **SS-dithiol**. The black arrow in the figures indicates the elongation temperature (T_e) in a two-step nucleation elongation process. (d) Plot of Te of the co-assembled solution against varying **SS-dithiol** concentration while keeping **SS-diOEt** concentration constant. (e) Plot of T_e against different **SS-dithiol:SS-diOEt** molar ratio with a fixed total concentration at 3×10^{-5} M. Green dots and red dots in figures (d) and (e) corresponds to the T_e obtained by monitoring the **SS-diOEt** and **SS-dithiol** spectral features, respectively. (f) SIM microscopy image of the co-assembled solution of **SS-diOEt** and **SS-dithiol** contains alternating green, red emitting fibers which depicts formation of supramolecular BCPs. Corresponding intensity profile of the fibers in green, red, and merged channel illustrates that the green and red emission does not overlay with each other's. The white oval shapes represent the fibers from where the intensity profiles were extracted. ([**SS-diOEt**] = [**SS-dithiol**] = 2.5×10^{-5} M, TCE/MCH, 25/75 (v/v), l = 10 mm, (green channel: λ_{ex} = 488 nm, λ_{coll} = 495–575 nm), (red channel: λ_{ex} = 561 nm, λ_{coll} = 570–650 nm)).

Supramolecular block copolymerization under thermodynamic control

Having investigated the mechanistic aspects of supramolecular homopolymerization of both **SS-dithiol** and **SS-diOEt** monomers, we next attempted the supramolecular block copolymerization process to construct the axial organic heterostructures. In general, experimentally we could observe that **SS-dithiol** forms stable supramolecular homopolymers under thermodynamic conditions (Figure 1g) while **SS-diOEt** tends fall into a kinetically trapped metastable phase (Figure S11a) prior to time-dependent supramolecular homopolymerization process (Figure 1h). Thus, first we attempted the heterogeneous seeded supramolecular polymerization under kinetic control to construct multi-component block topology.[15] However, the introduction of **SS-dithiol** seeds into the metastable state of **SS-diOEt** (Figure S13) does not trigger an immediate growth of later, which ruled out the possibility of heterogeneous nucleation process of the monomers under kinetic control. We speculate this could be due to the slower dynamics (at room temperature) of **SS-diOEt** monomers and to their higher free-energy of monomer-monomer interactions compared to that of hetero-monomeric interactions (see Figure 1i). This would make **SS-diOEt** monomers that exchange out of the **SS-diOEt** assemblies into the solution more prone to re-assemble with other **SS-diOEt** monomers (or to reassemble back onto **SS-diOEt** assemblies) rather than to stack onto **SS-dithiol** assemblies (Figure S14).

We envision that supramolecular copolymerization of the monomers under thermodynamic control[22], analogous to the classical chain copolymerization, would be another strategy to achieve block microstructure. Furthermore, the reactivity ratio (R) of 1.17 that can be calculated from the interaction free-energies of Figure 1i ($R = (\Delta G_{\text{SS-dithiol-SS-dithiol}} + \Delta G_{\text{SS-diOEt-SS-diOEt}})/2\times\Delta G_{\text{SS-dithiol-SS-diOEt}}$) obtained from the CG simulations suggests the possibility of generating a blocky organization during a cooperative supramolecular copolymerization. We have utilized the distinct green (λ_{max} = 505 nm) and red (λ_{max} = 575 nm) emission of **SS-diOEt** and **SS-dithiol** monomers, respectively, which could also be selectively excited, to spectroscopically probe the supramolecular copolymerization process (Figure S15).

In a typical supramolecular copolymerization process under thermodynamic conditions, a 1:1 mixture (c = 2.5×10^{-5} M) of **SS-diOEt** and **SS-dithiol** in 25 % TCE in MCH (v/v) solvent mixture was heated to 363 K and cooled under thermodynamic control at a rate of 1 K/min (Figure 2a). Temperature-dependent emission changes of a 1:1 mixture of **SS-dithiol** and **SS-diOEt** obtained via selective excitation (λ_{ex} = 430 nm for **SS-diOEt** and 530 nm for **SS-dithiol**) and monitoring at 490 nm and 57o nm for **SS-dithiol** and **SS-diOEt**, respectively indicated the co-assembly between the two components (Figure 2b and 2c). Temperature-dependent emission changes of **SS-dithiol** showed a two-step non-linear changes (Figure 2c), with a linear region with no change in degree of aggregation followed by a nonlinear change in degree of aggregation on reaching the critical temperature (marked with black arrow in Figure 2b, c). This two-step nonlinear changes could be fitted to a cooperative nucleation-elongation model. Interestingly, the T_e of 325 K of the 1:1 monomeric mixture matches well with that of **SS-dithiol** homopolymer at the same concentration (T_e = 325 K, c = 2.5×10^{-5} M) (Figure 2c). More importantly, the selective probing of the **SS-diOEt** emission during co-assembly (Figure 2b), also followed a nucleation-elongation mechanism with identical T_e (325 K) as that of **SS-dithiol**, despite the fact that **SS-diOEt** homopolymer at same concentration get trapped into a metastable state under similar conditions (Figure S11a). This provides a clear indication of heterogeneous nucleation and supramolecular copolymerization process of **SS-dithiol** and **SS-diOEt** monomers (Figure 2b). Supramolecular copolymerization of **SS-diOEt** and **SS-dithiol** mixtures with constant **SS-diOEt** (c = 2.5×10^{-5} M) and varying **SS-dithiol** (1.5×10^{-5} to 4×10^{-5} M) concentrations, showed a decrease in T_e of the supramolecular copolymer with a decrease in **SS-dithiol** concentration (Figure 2d, S16a, S16b and S17). Further, on the variation of monomer ratio (**SS-dithiol:SS-diOEt** from 9:1 to 1:9) by keeping the total concentration constant (3×10^{-5} M), (Figure 2e, S16c, S16d and S17) showed a linear decrease in T_e proportional with the decrease in the **SS-dithiol** concentration. These observations clearly indicate the heterogeneous nucleation of **SS-diOEt** on **SS-dithiol** nuclei rather than a cooperative alternating copolymerization of a heterodimer.

Visualization of the co-assembled solution using SIM microscopy (upon selective excitation and probing through different emission channels) revealed blocky supramolecular polymers with alternating green and red segments of stacked **SS-diOEt** and **SS-dithiol** monomers, respectively (Figure 2f and S20). Since **SS-dithiol** also gets excited at the **SS-diOEt** excitation (green channel) due to its broad absorption (Figure S7), we observe a continuous green-emitting chain in green channel due to the contribution from both monomers. However, the low photo luminescence emission of **SS-dithiol (**upon excitation in green channel) expected to provide a low green intensity in **SS-dithiol** segment as compared to the highly intense green emission from the **SS-diOEt** blocks. This is exactly observed from the green intensity profile over a micrometer long fiber, which showed a variation in green emission depending on the nature of segments (Figure 2f). Additionally, visualizing through the red channel and corresponding intensity profiles selectively confirmed the presence of red **SS-dithiol** segment. Complementary nature of red and green intensity profiles from the merged channel unequivocally proved the presence of an alternate segmental organization. Blocky organization of the components in the supramolecular copolymer rather than an alternating monomer sequence originates from the lower hetero-free energy gain ($\Delta G_{\text{SS-diOEt-SS-dithiol}}$) compared to the total homo-free energy gain ($\Delta G_{\text{SS-diOEt-SS-diOEt}}$, $\Delta G_{\text{SS-dithiol-SS-dithiol}}$), as reported by Meijer and coworkers (*vide supra*).[22] Melting temperature (T_m) obtained from the heating curve of the supramolecular block copolymer (heating rate = 1 K/min) shows an increase in stability of **SS-diOEt** segment from 322 K to 335 K (Figure S21a) and a decrease in stability of **SS-dithiol** segment from 341 K to 334 K (Figure S21b), compared to the corresponding pure components at similar concentrations.

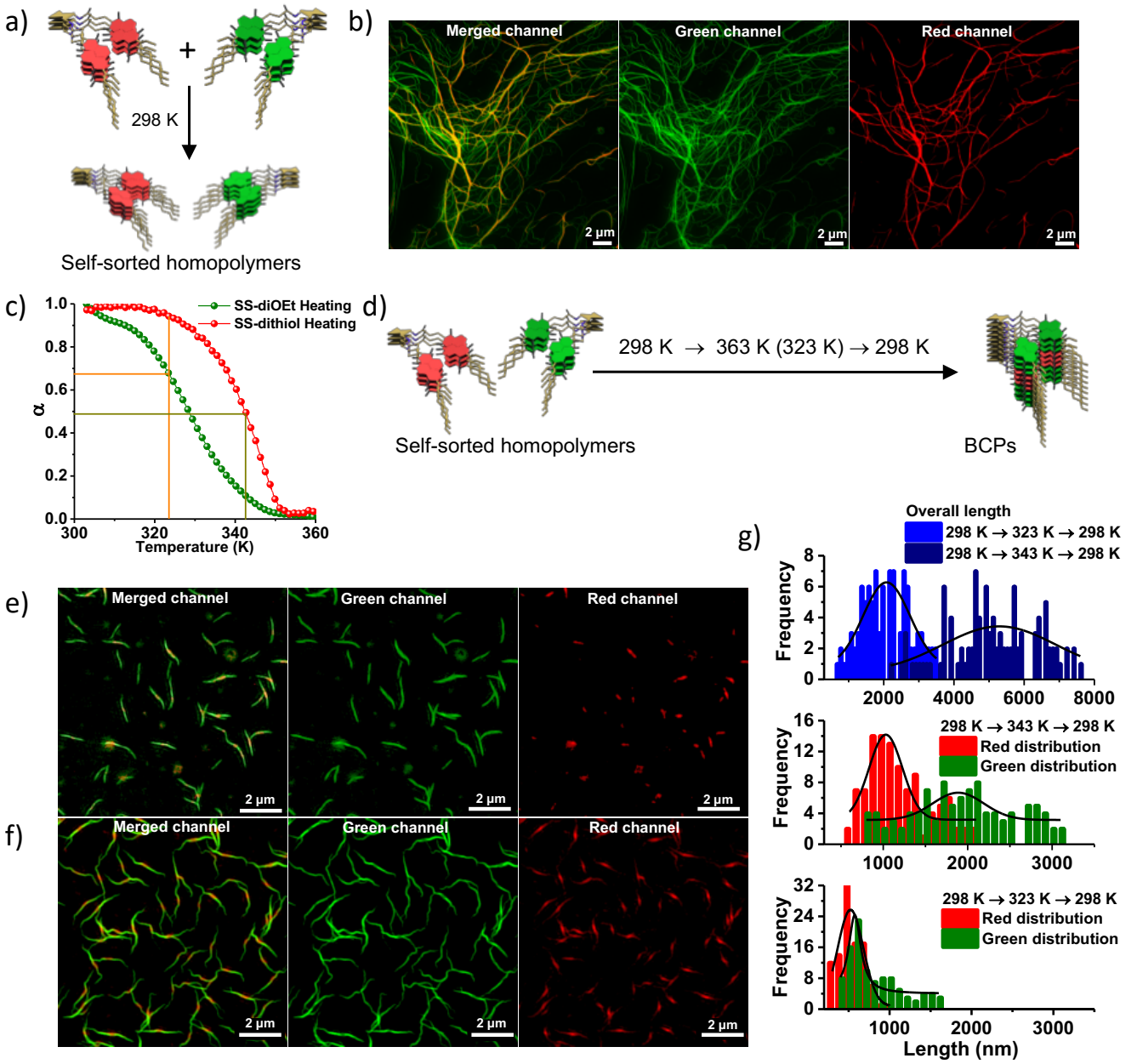

Figure 3. Distribution Analyses of Tri-block Microstructures: (a) Schematic illustration and (b) SIM images of post-synthetically mixed **SS-diOEt** and **SS-dithiol** homopolymers in green, red and merged channels, showing narcissistically self-sorted stacks. (c) Heating curves of the supramolecular homopolymers of **SS-diOEt** and **SS-dithiol** (c = 2.5×10^{-5} M, 1K/min heating rate) obtained by probing the temperature-dependent absorbance changes at 480 nm for **SS-diOEt** and 550 nm for **SS-dithiol**; which shows higher stability for **SS-dithiol** in comparison to **SS-diOEt** stacks. (d) Schematic illustration of the annealing induced re-organization of self-sorted homopolymers to tri-BCPs by slow cooling form 343 K and 323 K. SIM microscopy images of BCPs in green, red and merged channel obtained via annealing from (e) 323 K and (f) 343 K (heating rate = cooling rate = 1 K/min). (g) Contour length distribution analyses showing the average lengths of the BCPs (above) and both green and red blocks, upon the annealing process from 323 K and 343 K to 298 K. In each case, 100 individual BCP chains were counted to construct the distribution. ([**SS-diOEt**] = [**SS-dithiol**] = 2.5×10^{-5} M, TCE/MCH, 25/75 (v/v), l = 10 mm, (green channel: λ_{ex} = 488 nm, λ_{coll} = 495–575 nm), (red channel: λ_{ex} = 561 nm, λ_{coll} = 570–650 nm))

Annealing induced modulation of block length distribution

Mixing of the supramolecular homopolymers of **SS-diOEt** and **SS-dithiol** (c = 2.5×10^{-5} M, TCE/MCH, 25/75 (v/v)) at room temperature results in narcissistically self-sorted green and red chains (Figure 3a) as evident from SIM microscopic images (Figure 3b, S22 and S23). The self-sorted supramolecular stacks remain intact with time at room temperature, as evident from the spectroscopic and microscopic studies performed after two days, suggesting that these systems are less dynamic at ro0m temperature (Figure S24). This observation is further consistent with the CG MetaD simulations, which revealed a slow monomer exchange dynamics, especially in the **SS-diOEt**

stacks with the solvent, compared to similar stacks reported in the literature,[17a] which in this case can be also computed to the monomer conformational transitions associated with the exchange process (Figure 1j). However, heating curves of **SS-diOEt** and **SS-dithiol** supramolecular homopolymers at similar concentrations (c = 2.5×10^{-5} M) showed differential stability, with higher melting temperature (T_m) for **SS-dithiol** (T_m= 342 K) stacks compared to the assemblies of **SS-diOEt** (T_m = 328 K) (Figure 3c and S25). The lower stability of **SS-diOEt** supramolecular homopolymers seen in the experiments can be attributed to the intrinsically more disordered nature (in terms of the internal organization of the monomers). In fact, a detailed analysis of the internal ordering of these fibers inferred from the MD simulations indicate the presence of defects along the stacks,[32c,33] while these are more present in **SS-diOEt** than in **SS-dithiol** (*vide supra*).

Further, we anticipated that the difference in the extent of melting of two homopolymers at a higher temperature would lead to differential exchange dynamics for the two segments, and hence cooling down from high temperatures would affect the length distribution of the blocky segments in the resulting supramolecular copolymers. Interestingly on cooling the self-sorted solution of the homopolymers from (heating and cooling rate = 1 K/min) 323 K and **343** K to room temperature leads to the formation of isolated supramolecular BCP chains (Figure S26 and S27) as evident from the SIM images (Figure 3e and 3f). Large number of isolated chains in the SIM image allowed us to perform an unprecedented statistical analysis on dynamic supramolecular BCPs to extract the degree of polymerization, block lengths, and dispersity similar to studies performed on polymeric blocky cylindrical micelles.[8,9] CLD analyses (Figure 3g) showed that the supramolecular BCPs formed by the annealing showed excellent dispersity and length control as evident from the weight average length (L_w), number average length (L_n), and the polydispersity index (PDI). The overall length of the supramolecular BCP chains obtained by annealing from 323K was calculated to be 2090 nm (L_n) and 2322 nm (L_w) with a PDI of 1.11 (Table S11). On the other hand, stacks obtained by annealing from 343 K showed an increase in the degree of polymerization as evident from the increased L_n and L_w of 5075 nm and 5393 nm, respectively with a PDI of 1.06 (Table S11). A similar trend was also observed in the length distribution of both green and red block segments. L_n and L_w values for green blocks (**SS-diOEt)** in the supramolecular block copolymer annealed from 323 K, was calculated to be 800 nm and 935 nm (PDI~ 1.16), whereas the red blocks (**SS-dithiol)** exhibited L_n and L_w values of 540 nm and 581 nm (PDI~1.07), respectively (Figure 3g, Table S11 and S12). However, in supramolecular BCPs from 343 K, the length of both blocks was increased leading to an increase in the overall length of the multi-component stacks (Green: L_n = 1915 nm, L_w = 2115 nm, PDI = 1.10; Red: L_n = 1195 nm, L_w = 1306 nm, PDI = 1.09) (Table S11 and S12).

It is worth noting that both the number and weight average lengths of the green (**SS-diOEt)** blocks are always higher than that of the red blocks (**SS-dithiol)** in the supramolecular block copolymers (Figure 3g). We envisage that this could be due to the significantly higher interactions between the monomers of **SS-diOEt** compared to that of **SS-dithiol** monomers (Figure 1i). This is like the chain copolymerization process of covalent systems, where higher reactivity of one of the monomers leads to the larger block length of that monomer. The length distribution analysis could not be measured for the extended supramolecular blocky copolymers obtained via the cooperative growth from the monomeric state at 363 K (Figure 2) due to the entangled network of green and red segments.

Directional energy harvesting in axial organic heterostructures

As there is a considerable amount of overlap between the emission spectrum of **SS-diOEt** (energy donor) and the absorption spectrum of **SS-dithiol** (energy acceptor) monomers organized in the supramolecular block copolymers, we anticipated energy migration along the π-stacked chromophores organized along the fibers.[24] Indeed, the solution phase emission spectrum of these supramolecular donor-acceptor BCPs, when the donor monomers are excited (at 430 nm), showed a quenching of donor emission (λ_{max} = 510 nm) and a concomitant two-fold enhancement of the acceptor emission (λ_{max} = 560 nm) with respect to (direct) excitation of the acceptor at 530 nm (Figure S19). Such amplification in acceptor emission along with the quenching of the donor emission indicates the possibility of mesoscale excitation-energy migration[24] and energy transfer between adjacent donor-acceptor block segments.

The segmented arrangement of donors and the acceptor domains within a single supramolecular BCP can be called as organic axial nano-heterostructures with linear donor-acceptor interface or junctions, reminiscent of well-studied class of inorganic axial heterostructures.[26] To investigate excitation energy migration between adjacent donor and acceptor blocks, we performed spectrally-resolved fluorescence microscopy of individual block copolymerized (BCP) heterostructures. A representative energy-mapped pseudo-color image (Section B.2.1. supporting information) shows two spatially segregated BCP fibrils, BCP-1, and BCP-2 (Figure 4a (ii and iii)), which clearly depict the alternating segment distribution of donor and acceptor blocks within individual fibrils. It is important to mention that, when excited–at 405 nm, the donor segments (green) within the BCP fibrils have extremely feeble fluorescence, in stark contrast to donor-only (homopolymer) fibrils where the emission is (typically) at least an order of magnitude higher when imaged under identical conditions (Figure S29). The dramatic quenching of donor emission provides some indirect evidence of excitation energy migration from the donor blocks to adjacent acceptor blocks within the BCP fibrils. To thoroughly investigate energy transfer (or excitation energy migration) between donor and acceptor blocks, we performed dual-excitation sensitized emission imaging (Section B2.1. supporting information) of individual BCP heterostructures.[37] This was achieved by detecting the acceptor emission (545-635 nm) for a single fibril (BCP-3) via sequential excitation of the acceptors (at $\lambda_{Ex}^{A} = 532\ nm$) and the donors (at $\lambda_{Ex}^{D} = 405\ nm$).

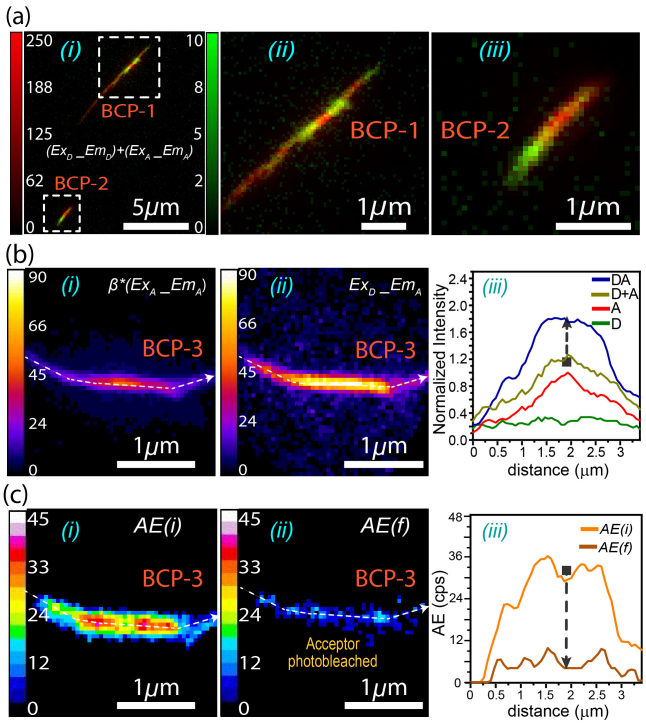

Figure 4. Light-Harvesting Organic Heterostructures: Spectrally-resolved fluorescence images of individual supramolecular block copolymers (BCPs). (a) Pseudocolor energy mapped fluorescence image of spatially-isolated single BCP fibrils (*i*). Blowup of two representative fibrils, BCP-1 (*ii*) and BCP-2 (*iii*). (b) Expected emission intensity of acceptors in BCP-3 fibril upon excitation at 405 nm, if there is no sensitization (*i*), and the observed (enhanced) emission of acceptors from in BCP-3 fibril. The corresponding normalized intensity line profiles along BCP-3 (b(*iii*)), for A-channel emission via 405 nm excitation of donors and acceptors (D, A) their cumulative intensity (D+A), and sensitized emission (enhancement) owing to energy transfer (DA). Image depicting acceptor intensity enhancement (AE) of BCP-3 (c) prior to (*i*) and post (*ii*) acceptor photobleaching, along with the corresponding AE line profiles (*iii*).

First, we obtained a fluorescence intensity image of BCP-3 via excitation of acceptors (at $\boldsymbol{\lambda_{Ex}^{A}}$), which was then factorized by the ratio of the extinction coefficients ($\beta = \varepsilon_{405}/\varepsilon_{532}$) of the acceptor when excited at 405 nm ($\boldsymbol{\lambda_{Ex}^{D}}$) and at 532 nm ($\boldsymbol{\lambda_{Ex}^{A}}$) (verified by imaging acceptor-only homopolymers, see Figure S30). This operation over the image yields spatially-resolved emission intensities of acceptors in the absence of any sensitization (Figure 4b(i)), had they been excited at $\boldsymbol{\lambda_{Ex}^{D}}$. In effect, Figure 4b(i) portrays the maximum emission intensity of acceptors along the fibril if there is no energy transfer. However, upon excitation of the donors in the BCP fibrils, we find significantly enhanced (sensitized) emission from the acceptors (Figure 4b(ii)). Such augmentation of emission in the acceptor segment, as portrayed in the spatial distribution of intensities of BCP-3 (Figure 4b(iii)), serves as an unambiguous indicator of excitation energy transfer from flacking donor blocks to the central acceptor block in single BCP fibrils.

The sensitized fluorescence image of BCP-3 (Figure 4c(i)) depicts the acceptor intensity enhancement (AE) due to energy transfer from donors **(**see method B.2.2. supporting information**).** Interestingly, we find substantial spatial non-uniformity in the AE for a single BCP fibril; for instance, the central region of BCP-3 has considerably lower sensitized emission owing to the absence of the donors within the acceptor segment as compared to that in the interface regions where both donors and acceptors are present. Nonetheless, substantial AE observed over the entire acceptor block (Figure 4c (*i*, *iii*)) indicates transfer of excitation energy from flanking donor blocks located over more than several hundred nanometers apart. In addition, we checked with narcissistically self-sorted donor and acceptor supramolecular stacks and observed significant AE only at regions where both fibrils are in contact due to the close proximity of donors and acceptors (Figure S31). Further, to verify whether the observed enhancement of acceptor emission (Figure 4c(i)) indeed owes to excitation migration from the donor segments,[37] we selectively photo-bleached the acceptors of BCP-3 using intense 532 nm laser excitation (Section B.2.1. supporting information).[38] We find that upon progressive irreversible photo-bleaching of acceptors, there is a concurrent enhancement in the emission of donors when exited at 405 nm (Figure S32), owing to the unavailability of enough acceptors to transfer their excitation energy. As a consequence, the resulting sensitized emission image of BCP-3 post acceptor photobleaching (Figure 4c(ii)) shows nominal AE. It is relevant to mention that spatially-resolved fluorescence spectroscopy measurements (Section B.2.3. supporting information) on single BCP heterostructures (Figure S33) further validate the inferences of the above dual-excitation sensitized emission imaging, and therefore provides direct support to the hypothesis of energy migration between adjacent segments within individual block copolymers.

Conclusion

In conclusion, we have explored the cooperative supramolecular block copolymerization of optically distinct cNDI monomers with slightly different substituents at the core for the synthesis of the light-harvesting organic heterostructure. The characteristic and distinct optical properties of cNDI derivatives, which are sensitive to intermolecular interactions aided the spectroscopic probing of the microstructure during thermodynamically driven supramolecular copolymerization. Distinct green and red fluorescence of the **SS-diOEt** and **SS-dithiol** stacked monomers, respectively facilitated the structural characterization of multi-block microstructure of these supramolecular BCPs via the visualization through SIM-based super resolution imaging. Furthermore, the effective fluorescence imaging allowed a unique size distribution analysis of individual blocks which showed a narrow polydispersity with a PDI of 1.1. The free-energy data for the **SS-dithiol** and **SS-diOEt** intermixing and the comprehension of the exchange mechanisms in these BCPs obtained from the CG simulations helped us in rationalizing the experimental results. A detailed computational study of the exchange mechanism and of defects inside these fibers helped us to rationalize the dynamic behavior of these assemblies and their dynamic tendency/limitation to co-assemble. Finally, spectrally resolved FRET-based microscopy studies on single BCP chains, showed directional light-harvesting along the axial hetero-junctions, thus demonstrating its remarkable potential as functional organic heterostructures.

Supramolecular block copolymerization presented here from the monomeric state of components follows a nucle-

ation-elongation mechanism and hence is reminiscent of classical chain-growth copolymerization of covalent polymers, where blocky organization of monomers is determined by the reactivity ratio of monomers. We envisage that this synthetic strategy can be generalized for the construction of a variety of axial organic heterostructures with stable segmented microstructure for diverse optoelectronic applications, charge transport and catalysis.

ASSOCIATED CONTENT

Supporting Information

Synthetic Schemes, procedures, supporting experimental figures, characterization spectra, extended computational methods and procedures. This material is available free of charge via the Internet at http://pubs.acs.org."

AUTHOR INFORMATION

*Corresponding Author

*george@jncasr.ac.in

*arindam@chem.iitb.ac.in

*giovanni.pavan@polito.it

*sagasti@jncasr.ac.in

Author Contributions

The manuscript was written through contribution of all authors. All authors have given approval to the final version of the manuscript

ACKNOWLEDGMENT

We thank Prof. C. N. R. Rao, FRS for his support and guidance. We would also like to thank JNCASR and the Department of Science and Technology, Government of India, for financial support. S. J. G. acknowledges the funding received from Department of Biotechnology, Government of India for the Indo-Switzerland Joint Research project (BT/IN/Swiss/55/SJG/2018-2019). A.S., R.S. and T.B. thanks CSIR for fellowship. G. M. P. acknowledges the funding received by the Swiss National Science Foundation (SNSF grants IZLIZ2_183336) and by the European Research Council (ERC) under the European Union's Horizon 2020 research and innovation programme (grant agreement no. 818776 - DYNAPOL). This work was supported by a grant from the Swiss National Supercomputing Centre (CSCS) under project ID s934. Further computational resources were provided by HPC@POLITO, a project of Academic Computing within the Department of Control and Computer Engineering at the Politecnico di Torino (http://www.hpc.polito.it).

ABBREVIATIONS

AE, acceptor intensity enhancement.

REFERENCES

(1) (a) De Greef, T. F. A.; Smulders, M. M. J.; Wolffs, M.; Schenning, A. P. H. J.; Sijbesma, R. P.; Meijer, E. W. Supramolecular polymerization. *Chem. Rev.* **2009**, *109*, 5687–5754. (b) de Greef, T. F. A.; Meijer, E. W. Supramolecular polymers. *Nature* **2008**, *453*, 171-173. (c) Aida, T.; Meijer, E. W.; Stupp, S. I. Functional Supramolecular Polymers. *Science* **2012**, *335*, 813-817. (d) Vantomme, G.; Meijer, E. W. The construction of supramolecular systems. *Science* **2019**, *363*, 1396-1397. (e) Aida, T. On Supramolecular Polymerization: Interview with Takuzo Aida. *Adv. Mater.* **2019**, 1905445. (f) Aida, T.; Meijer, E. W. Supramolecular Polymers – we've Come Full Circle. *Isr. J. Chem.* **2020**, *60*, 33–47.

(2) (a) Adelizzi, B.; Van Zee, N. J.; De Windt, L. N.; Palmans, A. R.; Meijer, E. W. Future of supramolecular copolymers unveiled by reflecting on covalent copolymerization. *J. Am. Chem. Soc.* **2019**, *141*, 6110-6121. (b) Wehner, M.; Würthner, F. Supramolecular polymerization through kinetic pathway control and living chain growth. *Nat. Rev. Chem.* **2020**, *4*, 38-53. (c) Besenius, Pol. Controlling supramolecular polymerization through multicomponent self-assembly. *Polymer Chemistry* **2017**, *55*, 34–78.

(3) (a) Jain, A.; George, S. J. New directions in supramolecular electronics. *Mater. Today* **2015**, *18*, 206-214. (b) Jain, A.; George, S. J. Meshing organic nanowires. *Nat. Nanotech.* **2016**, *11*, 843-844.

(4) (a) Lutz, J. F.; Ouchi, M.; Liu, D. R.; Sawamoto, M. Sequence controlled polymers. *Science* **2013**, *341*, 1238149. (b) Schacher, F. H.; Rupar, P. A.; Manners, I. Functional block copolymers: nanostructured materials with emerging applications. *Angew. Chem., Int. Ed.* **2012**, *51*, 7898–7921.

(5) (a) Frisch, H.; Unsleber, J. P.; Lgdeker, D.; Peterlechner, M.; Brunklaus, G.; Waller, M.; Besenius, P. pH-Switchable ampholytic supramolecular copolymers. *Angew. Chem., Int. Ed.* **2013**, *52*, 10097–10101. (b) Frisch, H.; Fritz, E.; Stricker, F.; Schmüser, L.; Spitzer, D.; Weidner, T.; Ravoo, B. J.; Besenius, P. Kinetically con-trolled sequential growth of surface-grafted chiral supramolecular copolymers. *Angew. Chem., Int. Ed.* **2016**, *55*, 7242 – 7246. (c) Zhang, X.; Wang, C. Supramolecular amphiphiles. *Chem. Soc. Rev.* **2011**, *40*, 94-101. (d) Wang, C.; Guo, Y.; Wang, Y.; Xu, H.; Wang, R.; Zhang, X. Supramolecular amphiphiles based on a water-soluble charge-transfer complex: fabrication of ultralong nanofibers with tunable straightness. *Angew. Chem., Int. Ed.* **2009**, *48*, 8962–896. (e) Appel, E. A.; Biedermann, F.; Rauwald, U.; Jones, S. T.; Zayed, J. M.; Scherman, O. A. Supramolecular cross-linked networks via host guest complexation with cucurbit[8]uril. *J. Am. Chem. Soc.* **2010**, *132*, 14251-14260.

(6) (a) Van Gestel, J.; Palmans, A. R. A.; Titulaer, B.; Vekemans, J. A. J. M.; Meijer, E. W. "Majority-Rules" operative in Chiral Columnar Stacks of C3-Symmetrical Molecules. *J. Am. Chem. Soc.* **2005**, *127*, 5490–5494. (b) Smulders, M. M. J.; Schenning, A. P. H. J.; Meijer, E. W. Insight into the Mechanisms of Cooperative Self-Assembly: The "Sergeants-and-Soldiers" Principle of Chiral and Achiral C3-Symmetrical Discotic Triamides. *J. Am. Chem. Soc.* **2008**, *130*, 606–611. (c) Jin, W.; Fukushima, T.; Niki, M.; Kosaka, A.; Ishii, N.; Aida, T. Self-Assembled Graphitic Nanotubes with One-Handed Helical Arrays of a Chiral Amphiphilic Molecular Graphene. *Proc. Natl. Acad. Sci.* **2005**, *102*, 10801–10806. (d) Helmich, F.; Smulders, M. M. J.; Lee, C. C.; Schenning, A. P. H. J.; Meijer, E. W. Effect of Stereogenic Centers on the Self-Sorting, Depolymerization, and Atropisomerization Kinetics of Porphyrin-Based Aggregates. *J. Am. Chem. Soc.* **2011**, *133*, 12238–12246. (e) Kim, T.; Mori, T.; Aida, T.; Miyajima, D. Dynamic Propeller Conformation for the Unprecedentedly High Degree of Chiral Amplification of Supramolecular Helices. *Chem. Sci.* **2016**, *7*, 6689–6694. (f) Ajayaghosh, A.; Varghese, R.; George, S. J.; Vijayakumar, C. Transcription and Amplification of Molecular Chirality to Oppositely Biased Supramolecular π Helices. *Angew. Chem., Int. Ed.* **2006**, *45*, 1141–1144. (g) García, F.; Sánchez, L. Structural Rules for the Chiral Supramolecular Organization of OPEbased Discotics: Induction of Helicity and Amplification of Chirality. *J. Am. Chem. Soc.* **2012**, *134*, 734–742. (h) Smulders, M. M. J.; Stals, P. J. M.; Mes, T.; Paffen, T. F. E.; Schenning, A. P. H. J.; Palmans, A. R. A.; Meijer, E. W. Probing the Limits of the Majority-Rules Principle in a Dynamic Supramolecular Polymer. *J. Am. Chem. Soc.* **2010**, *132*, 620–626. (i) Coelho, J. P.; Matern, J.; Albuquerque, R. Q.; Fernández, G. Mechanistic Insights into Statistical Co-Assembly of Metal Complexes. *Chem. Eur. J.* **2019**, *25*, 8960-8964.

(7) (a) Yagai, S.; Hamamura, S.; Wang, H.; Stepanenko, V.; Seki, T.; Unoike, K.; Kikkawa, Y.; Karatsu, T.; Kitamura, A.; Würthner, F. Unconventional Hydrogen-Bond-Directed Hierarchical Co-Assembly between Perylene Bisimide and Azobenzene-Functionalized Melamine. *Org. Biomol. Chem.* **2009**, *7*, 3926–3929. (b) Görl, D.; Zhang, X.; Stepanenko, V.; Würthner, F. Supramolecular Block Copolymers by Kinetically Controlled Co-Self-Assembly of Planar and Core-Twisted Perylene Bisimides. *Nat. Commun.* **2015**, *6*, 7009.

(8) (a) Wang, X.; Guerin, G.; Wang, H.; Wang, Y.; Manners, I.; Winnik, M. Cylindrical block copolymer micelles and co-micelles of controlled length and architecture. *Science* **2007**, *317*, 644–648. (b) Gilroy, J. B.; Gädt, T.; Whittell, G. R.; Chabanne, L.; Mitchels, J. M.; Richardson, R. M.;

Winnik, M. A.; Manners, I. Monodisperse cylindrical micelles by crystallization-driven living self-assembly. *Nat. Chem.* **2010**, *2*, 566–570. (c) Hailes, R. L. N.; Oliver, A. M.; Gwyther, J.; Whittell, G. R.; Manners, I. Polyferrocenylsilanes: synthesis, properties, and applications. *Chem. Soc. Rev.,* **2016**, *45*, 5358.

(9) (a) Gädt, T.; Ieong, N. S.; Cambridge, G.; Winnik, M. A.; Manners, I. Complex and hierarchical micelle architectures from diblock copolymers using living, crystallization-driven polymerizations. *Nat. Mater.* **2009**, *8*, 144. (b) Hudson, Z. M.; Boott, C. E.; Robinson, M. E.; Rupar, P. A.; Winnik, M. A.; Manners, I. Tailored hierarchical micelle architectures using living crystallization-driven self-assembly in two dimensions. *Nat. Chem.* **2014**, *6*, 893; (c) He, X.; Hsiao, M.-S.; Boott, C. E.; Harniman, R. L.; Nazemi, A.; Li, X.; Winnik, M. A.; Manners, I. Two-dimensional assemblies from crystallizable homopolymers with charged termini. *Nat. Mater.* **2017**, *16*, 481. (d) Qiu, H.; Gao, Y.; Boott, C. E.; Gould, O. E. C.; Harniman, R. L.; Miles, M. J.; Webb, S. E. D.; Winnik, M. A.; Manners, I. Uniform patchy and hollow rectangular platelet micelles from crystallizable polymer blends. *Science* **2016**, *352*, 697. (e) Finnegan, J. R.; Lunn, D. J.; Gould, O. E. C.; Hudson, Z. M.; Whittell, G. R.; Winnik, M. A.; Manners, I. Gradient crystallization-driven self-assembly: cylindrical micelles with "patchy" segmented coronas via the coassembly of linear and brush block copolymers. *J. Am. Chem. Soc.* **2014**, *136*, 13835-13844. (f) Qiu, H.; Gao, Y.; An Du, V.; Harniman, R.; Winnik, M. A.; Manners, I. Branched micelles by living crystallization-driven block copolymer self-assembly under kinetic control. *J. Am. Chem. Soc.* **2015**, *137*, 2375–2385. (g) Nazemi, A.; He, X.; MacFarlane, L. R.; Harniman, R. L.; Hsiao, M.-S.; Winnik, M. A.; Faul, C. F. J.; Manners, I. Uniform "Patchy" Platelets by Seeded Heteroepitaxial Growth of Crystallizable Polymer Blends in Two Dimensions. *J. Am. Chem. Soc.* **2017**, *139*, 4409-4417.

(10) (a) Pal, A.; Malakoutikhah, M.; Leonetti, G.; Tezcan, M.; Colomb-Delsuc, M.; Nguyen, V.; van der Gucht, J.; Otto, S. Controlling the Structure and Length of Self-Synthesizing Supra-molecular Polymers through Nucleated Growth and Disassembly. *Angew.Chem. Int.Ed.* **2015**, *54*, 7852 –7856. (b) Wang, K.; Guo, Z.; Zhang, L.; Sun, K.; Yu, P.; Zhou, S.; Wang W.; Li, Z. Co-assembly of donor and acceptor towards organogels tuned by charge transfer interaction strength. *Soft Matter.* **2017**, *13*, 1948-1955. (c) Guo, Z.; Zhang, X.; Wang, Y.; Li, Z. Supramolecular Self-Assembly of Perylene Bisimide Derivatives Assisted by Various Groups. *Langmuir* **2019**, *35*, 342-358. (d) Ma, X.; Zhang, Y.; Zhang, Y.; Liu, Y.; Che, Y.; Zhao, J. Fabrication of Chiral-Selective Nanotubular Heterojunctions through Living Supramolecular Polymerization. *Angew. Chem., Int. Ed.* **2016**, *55*, 9539 –9543. (e) Liu, Y.; Peng, C.; Xiong, W.; Zhang, Y.; Gong, Y.; Che, Y.; Zhao, J. Two-Dimensional Seeded Self-Assembly of a Complex Hierarchical Perylene-Based Heterostructure. *Angew. Chem., Int. Ed.* **2017**, *56*, 11380 –11384.

(11) (a) Zhang, W.; Jin, W.; Fukushima, T.; Saeki, A.; Seki, S.; Aida, T. Supramolecular linear heterojunction composed of graphite-like semiconducting nanotubular segments. *Science* **2011**, *334*, 340–343. (b) Zhang, W.; Jin, W.; Fukushima, T.; Mori, T.; Aida, T. Helix sense-selective supramolecular polymerization seeded by a onehanded helical polymeric assembly. *J. Am. Chem. Soc.* **2015**, *137*, 13792–13795.

(12) Jung, S.H.; Bochicchio, D.; Pavan, G.M.; Takeuchi, M.; Sugiyasu, K. A block supramolecular polymer and its kinetically enhanced stability. *J. Am. Chem. Soc.* **2018**, *140*, 10570-10577.

(13) (a) Fukui, T.; Kawai, S.; Fujinuma, S.; Matsushita, Y.; Yasuda, T.; Sakurai, T.; Seki, S.; Takeuchi, M.; Sugiyasu, K. Control over differentiation of a metastable supramolecular assembly in one and two dimensions. *Nat. Chem.* **2017**, *9*, 493-499. (b) Ogi, S.; Sugiyasu, K.; Manna, S.; Samitsu, S.; Takeuchi, M. Living supramolecular polymerization realized through a biomimetic approach. *Nat. Chem.* **2014**, *6*, 188-195. (c) Ogi, S.; Stepanenko, V.; Sugiyasu, K.; Takeuchi, M.; Würthner, F. Mechanism of self-assem-bly process and seeded supramolecular polymerization of perylene bisimide organogelator. *J. Am. Chem. Soc.* **2015**, *137*, 3300-3307. (d) Dhiman, S.; George, S. J. Temporally controlled supramolecular polymerization. *Bull. Chem. Soc. Jpn.* **2018**, *91*, 687– 699. (e) Matern, J.; Dorca, Y.; Sánchez, L.; Fernández, G. Revising complex supramolecular polymerization under kinetic and thermodynamic control. *Angew. Chem., Int. Ed.* **2019**, *58*, 16730-16740. (f) van der Zwaag, D.; De Greef, T. F. A.; Meijer, E. W. Programmable supramolecular polymerizations. *Angew. Chem., Int. Ed.* **2015**, *54*, 8334–8336. (g) Mukhopadhyay, R. D.; Ajayaghosh, A. Living supramolecular polymerization. *Science* **2015**, *349*, 241. (h) Würthner, F. Living it up. *Nat. Chem.* **2014**, *6*, 171-173.

(14) (a) Mishra, A.; Korlepara, D. B.; Kumar, M.; Jain, A.; Jonnalagadda, N.; Bejagam, K. K.; Balasubramanian, S.; George, S. J. Biomimetic temporal self-assembly via fuel-driven controlled supramolecular polymerization. *Nat. Commun.* **2018**, *9*, 1295. (b) Jain, A.; Dhiman, S.; Dhayani, A.; Vemula, P. K.; George, S. J. Chemical fuel-driven living and transient supramolecular polymerization. *Nat. Commun.* **2019**, *10*, 450. (c) Ogi, S.; Stepanenko, V.; Thein, J.; Würthner, F. Impact of alkyl spacer length on aggregation pathways in kinetically controlled supramolecular polymerization. *J. Am. Chem. Soc.* **2016**, *138*, 670-678. (d) Ogi, S.; Matsumoto, K.; Yamaguchi, S. Seeded polymerization through the interplay of folding and aggregation of an amino-acid-based diamide. *Angew. Chem., Int. Ed.* **2018**, *57*, 2339–2343. (e) Greciano, E. E.; Matarranz, B.; Sánchez, L. Pathway complexity versus hierarchical self-assembly in N-annulated perylenes: Structural effects in seeded supramo-lecular polymerization. *Angew. Chem., Int. Ed.* **2018**, *57*, 4697–4701. (f) Endo, M.; Fukui, T.; Jung, S. H.; Yagai, S.; Takeuchi, M.; Sugiyasu, K. Photoregulated living supramolecular polymerization established by combining energy landscapes of photoisomerization and nucleation–elongation processes. *J. Am. Chem. Soc.* **2016**, *138*, 14347–14353. (g) Langenstroer, A.; Kartha, K. K.; Dorca, Y.; Droste, J.; Stepanenko, V.; Albuquerque, R. Q.; Hansen, M. R.; Sánchez, L.; Fernández G. Unraveling concomitant packing polymorphism in metallosupramolecular polymers. *J. Am. Chem. Soc.* **2019**, *141*, 5192–5200. (h) Wilkins, C. J.; He, X.; Symons, H. E.; Harniman, R. L.; Faul, C. F. J.; Manners, I. Living supramolecular polymerisation of perylene diimide amphiphiles by seeded growth under kinetic control. *Chem. Eur. J.* **2018**, *24*, 15556-15565. (i) Robinson, M. E.; Lunn, D. J.; Nazemi, A.; Whittell, G. R.; De Cola, L.; Manners, I. Length control of supramolecular polymeric nanofibers based on stacked planar platinum(ii) complexes by seeded-growth. *Chem. Commun.* **2015**, *51*, 3715921 –15924. (j) Aliprandi, A.; Mauro, M.; Cola, L. D. Controlling and imaging biomimetic self-assembly. *Nat. Chem.* **2016**, *8*, 10-15. (k) Kemper, B.; Zengerling, L.; Spitzer, D.; Otter, R.; Bauer, T.; Besenius, P. Kinetically controlled stepwise self-assembly of AuI-metallopeptides in water. *J. Am. Chem. Soc.* **2018**, *140*, 534-537.

(15) (a) Wagner, W.; Wehner, M.; Stepanenko, V.; Würthner, F. Supramolecular block copolymers by seeded living polymerization of perylene bisimides. *J. Am. Chem. Soc.* **2019**, *141*, 12044-12054. (b) Wagner, W.; Wehner, M.; Stepanenko, V.; Würthner, F. *CCS Chem.* **2019**, *1*, 598–613.

(16) (a) Sakai, N.; Mareda, J.; Vauthey, E.; Matile, S. Core-substituted Naphthalenediimides. *Chem., Commun.* **2010**, *46*, 4225-4237.

(17) (a) Sarkar, A.; Sasmal, R.; Empereur-mot, C.; Bochicchio, D.; Kompella, S. V. K.; Sharma, K.; Dhiman, S.; Sundaram, B.; Agasti, S. S.; Pavan, G. M.; George, S. J. Self-Sorted, Random, and Block Supramolecular Copolymers via Sequence Controlled, Multicomponent Self-Assembly. *J. Am. Chem. Soc.* **2020**, *142*, 7606-7617. (b) Wan, Q.; To, W-P.; Chang, X.; Che, C.-M. Controlled Synthesis of Pd^{II} and Pt^{II} Supramolecular Copolymer with Sequential Multiblock and Amplified Phosphorescence. *Chem*, **2020**, *6*, 1–23.

(18) (a) Lutz, J. F.; Lehn, J-M.; Meijer, E. W.; Matyjaszewski, K. From precision polymers to complex materials and systems. *Nat. Rev. Mater.* **2016**, *1*, 16024-16038. (b) Szwarc, M.; Nature 1956, 178, 1168–1169. (c) Matyjaszewski, K.; Xia, J. *Chem. Rev.* **2001**, *101*, 2921-2990.

(19) Odian, G. G. Principle of Polymerization, Third Ed.; Wiley, Ed.; 1991.

(20) (a) Kulkarni, C.; Balasubramanian, S.; George, S. J. What molecular features govern the mechanism of supramolecular polymerization? *ChemPhysChem* **2013**, *14*, 661 – 673. (b) Jonkheijm, P.; van der Schoot, P.; Schenning, A. P. H. J.; Meijer, E. W. Probing the solvent-assisted nucleation pathway in chemical self-assembly. *Science* **2006**, *313*, 80-83. (c) Kulkarni, C.; Bejagam, K. K.; Senanayak, P. S.; Narayan, K. S.; Balasubramanian, S.; George, S. J. Dipole-moment-driven cooperative supramolecular polymerization. *J. Am. Chem. Soc.* **2015**, *137*, 3924-3932.

(21) Kitamoto, Y.; Pan, Z.; Prabhu, D. D.; Isobe, A.; Ohba, T.; Shimizu, N.; Takagi, H.; Haruki, R.; Adachi, S. I.; Yagai, S. One-shot preparation of topologically chimeric nanofibers via a gradient supramolecular copolymerization. *Nat. Commun.* **2019**, *10*, 4578.

(22) Adelizzi, B.; Aloi, A.; Markvoort, A. J.; Ten Eikelder, H. M.; Voets, I. K.; Palmans, A. R.; Meijer, E. W. Supramolecular block copolymers under thermodynamic control. *J. Am. Chem. Soc.* **2018**, *140*, 7168-7175.

(23) Adelizzi, B.; Aloi, A.; Van Zee, N. J.; Palmans, A. R. A.; Meijer, 939E. W.; Voets, I. K. Painting Supramolecular Polymers in Organic Solvents by Super-resolution Microscopy. *ACS Nano* **2018**, *12*, 4431–9414439. (b) Kubota, R.; Nakamura, K.; Torigoe, S.; Hamachi, I. The Power of Confocal Laser Scanning Microscopy in Supramolecular Chem-istry: In situ real-time imaging of stimuli-responsive multi-compo-nent supramolecular hydrogels. *ChemistryOpen* **2020**, *9*, 67–79. (c) Albertazzi, L.; Zwaag, D. v. d.; Leenders, C. M. A.; Fitzner, R.; van der Hofstad, R. W.; Meijer, E. W. Probing Exchange Pathways in One-Dimensional Aggregates with Super-Resolution Microscopy. *Science* **2014**, *344*, 491-495.

(24) (a) Caram, J. R.; Doria, S.; Eisele, D. M.; Freyria, F. S.; Sinclair, T. S.; Rebentrost, P.; Lloyd, S.; Bawendi, M. G. Room-Temperature Micron-Scale Exciton Migration in a Stabilized Emissive Molecular Aggregate. *Nano Lett.* **2016**, *16*, 6808–6815. (b) Clark, K. A.; Krueger, E. L.; Vanden Bout, D. A. Direct Measurement of Energy Migration in Supramolecular Carbocyanine Dye Nanotubes. *J. Phys. Chem. Lett.* **2014**, *5*, 2274–2282. (c) Wittmann, B.; Wenzel, F. A.; Wiesneth, S.; Haedler, A. T.; Drechsler, M.; Kreger, K.; Köhler, J.; Meijer, E. W.; Schmidt, H. W.; Hildner, R. Enhancing Long-Range Energy Transport in Supramolecular Architectures by Tailoring Coherence Properties. *J. Am. Chem. Soc.* **2020**, *142*, 8323–8330. (d) Haedler, A. T.; Kreger, K.; Issac, A.; Wittmann, B.; Kivala, M.; Hammer, N.; Köhler, J.; Schmidt, H.-W.; Hildner, R. Long-range energy transport in single supramolecular nanofibres at room temperature. *Nature* **2015**, *9*, 196-200. (e) Wan, Y.; Stradomska, A.; Knoester, J.; Huang, L. Direct Imaging of Exciton Transport in Tubular Porphyrin Aggregates by Ultrafast Microscopy. *J. Am. Chem. Soc.* **2017**, *139*, 21, 7287-7293. (f) Brixner, T.; Hildner, R.; Köhler, J.; Lambert, C.; Würthner, F. Exciton Transport in Molecular Aggregates – From Natural Antennas to Synthetic Chromophore Systems. *Adv. Energy Mater.* **2017**, 1700236.

(25) Schenning, A. P. H. J.; Meijer, E. W. Supramolecular electronics; nanowires from self-assembled π-conjugated systems. *Chem. Commun.* **2005**, *26*, 3245–3258.

(26) (a) Yang, C.; Barrelet, C.J.; Capasso, F.; Lieber, C. M. Single p-Type/Intrinsic/n-Type Silicon Nanowires as Nanoscale Avalanche Photodetectors. *Nano Letters* **2006**, *6*, 2929-2934. (b) Tian, B.; Zheng, X.; Kempa, T. J.; Fang, Y.; Yu, N.; Yu, G.; Huang, J.; Lieber, C.M. Coaxial silicon nanowires as solar cells and nanoelec-tronic power sources. *Nature*, **2007**, *449*, 885-889. (c) Costi R.; Saunders E. A.; Elmalem E.; Salant A.; Banin, U. Visible Light-Induced Charge Retention and Photocatalysis with Hybrid CdSe–Au Nanodumbbells. *Nano Letters* **2008**, *8*, 637-641.

(27) Jin, X.; Price, M. B. Finnegan, J. R.; Boott, C. E.; Richter, J. M.; Rao, A.; Menke, S. M.; Friend, R. H.; Whittell, G. R.; Manners, I. Long-range exciton transport in conjugated polymer nanofibers prepared by-seeded growth. *Science* **2018**, *360*, 897-900.

(28) Hudson, Z. M.; Lunn, D. J.; Winnik, M. A.; Manners, I. *Nat. Commun.* **2014**, *5*, 3372.

(29) (a) Narayan, B.; Bejagam, K. K.; Balasubramanian, S.; George, S. J. Autoresolution of segregated and mixed p-n stacks by stereose-lective supramolecular polymerization in solution. *Angew. Chem., Int. Ed.* **2015**, *54*, 13245–13249. (b) Sarkar, A.; Dhiman, S.; Chalishazar, A.; George, S. J. Visualization of stereoselective supramolecular polymers by chirality-controlled energy transfer. *Angew. Chem., Int. Ed.* **2017**, *56*, 13767 –13771.

(30) (a) ten Eikelder, H. M. M.; Markvoort, A. J.; de Greef, T. F. A.; Hilbers, P. A. J. *J. Phys. Chem. B* **2012**, *116*, 5291. (b) Zhao, D.; Moore, J. S. Nucleation–elongation: a mechanism for cooperative supramolecular polymerization. *Org. Biomol. Chem.* **2003**, *1*, 3471-3491.

(31) (a) Oosawa, F.; Asakura, S. *Academic Press Inc., New York*, **1975**.

(32) (a) Bochicchio, D.; Pavan. G. M. Molecular modelling of supramolecular polymers. *Adv. Phys. X* **2018**, *3*, 1436408. (b) Bochicchio, D.; Pavan. G. M. From Cooperative Self-Assembly to Water-Soluble Supramolecular Polymers Using Coarse-Grained Simulations. *ACS Nano* **2017**, *11*, 1000-1011. (c) Gasparotto, P.; Bochicchio, D.; Ceriotti, M.; Pavan, G. M. Identifying and Tracking Defects in Dynamic Supramolecular Polymers. *J. Phys. Chem. B* **2020**, *124*, 589-599.

(33) Bochicchio, D.; Salvalaglio, M.; Pavan, G. M. Into the Dynamics of a Supramolecular Polymer at Submolecular Resolution. *Nat. commun.* **2017**, *8*, 1-11.

(34) Marrink, S. J.; Risselada, H. J.; Yefimov, S.; Tieleman, D. P.; De Vries, A. H. The MARTINI Force Field: Coarse Grained Model for Biomolecular Simulations. *J. Phys. Chem. B*, **2007**, *111*, 7812-7824.

(35) Barducci, A.; Bussi, G.; Parrinello, M. Well-tempered metadynamics: a smoothly converging and tunable free-energy method. *Physical review letters*, **2008**, *100*, 020603.

(36) Bochicchio, D.; Kwangmettatam, S.; Kudernac, T.; Pavan. G. M. How Defects Control the Out-of-Equilibrium Dissipative Evolution of a Supramolecular Tubule. *ACS Nano* **2019**, *13*, 4322-4334

(37) (a) Das, S.; Sharma, D. K.; Chakrabarty, S.; Chowdhury, A.; Sen Gupta, S. Bioactive Polymersomes Self-Assembled from Amphiphilic PPO-GlycoPolypeptides: Synthesis, Characterization, and Dual-Dye Encapsulation. *Langmuir* **2015**, *31*, 3402–3412. (b) Ray, S.; Singh, N.; Pandey, S.; Kumar, R.; Gadhe, L.; Datta, D.; Patel, K.; Mahato, J.; Navalkar, A.; Panigrahi, R.; Chatterjee, D.; Maiti, S.; Bhatia, S.; Mehra, S.; Singh, A.; Gerez, J.; Chowdhury, A.; Kumar, A.; Padinhateeri, R.; Riek, R.; Krishnamoorthy, G.; Maji, S.K. α-Synuclein aggregation nucleates through liquid-liquid phase separation. *Nature Chemistry* **2020**, *in press, doi:* 10.1038/s41557-020-0465-9.

(38) Berney, C.; Danuser, G. FRET or No FRET: A Quantitative Comparison. *Biophys J.* **2003**, **84**, 3992-4010

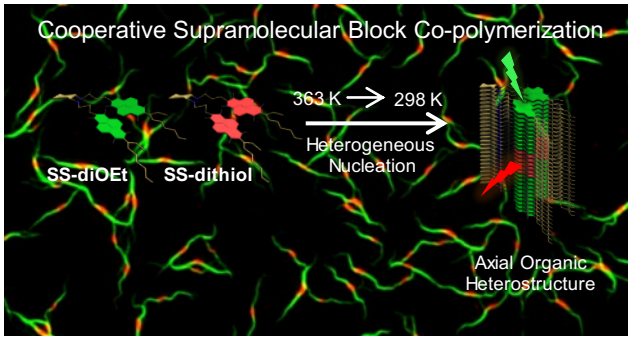

Table of Contents artwork